Fusion Engineering and Design 224 (2026) 115605

Contents lists available at ScienceDirect

Fusion Engineering and Design

journal homepage: www.elsevier.com/locate/fusengdes

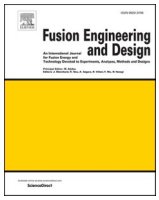

Demonstrating powder metallurgically produced long tungsten fiber-reinforced tungsten composite to serve as plasma-facing material

Yiran Mao [a,*], Jan Willem Coenen [a,b], Johann Riesch [c], Thomas Schwarz-Selinger [c], Elena Tejado [d], Arkadi Kreter [a], Alexis Terra [a], Marius Wirtz [a], Marcin Rasinski [a], Juan Du [e], Xiaoyue Tan [f], Yaohui Liu [g], Rudolf Neu [c,h], Christoph Broeckmann [g], Christian Linsmeier [a]

[a] Forschungszentrum Jülich GmbH, Institute of Fusion Energy and Nuclear Waste Management, Plasma Physics IFN-1, Germany
[b] Departmentof Engineering Physics, University of Wisconsin -Madison, USA
[c] Max-Planck-Institut für Plasmaphysik, Germany
[d] Departamento de Ciencia de los Materiales-CIME, Universidad Politécnica de Madrid, Spain
[e] Southwest Institute of Physics, China
[f] School of Mechanical Engineering, Hefei University of Technology, China
[g] Institut für Werkstoffanwendungen im Maschinenbau (IWM), RWTH Aachen University, Germany
[h] Technische Universität München, Germany

ARTICLE INFO

Keywords:
Plasma facing materials
Tungsten fiber reinforced tungsten composites
Plasma erosion
High flux tests
Hydrogen retention

ABSTRACT

For future fusion devices, tungsten is the main candidate materials for the application as plasma facing materials (PFMs). However, considering the challenging operational condition with high thermal loading/thermal stress combining plasma exposure and neutron irradiation/embrittlement, one of the major concern for tungsten as PFMs is its intrinsic brittleness. To avoid cracking and components failure, toughening tungsten is widely investigated, among which tungsten fiber reinforced tungsten composites (W_f/W) are developed using an extrinsic toughening mechanism. Recently, a new type of aligned long fiber W_f/W (L-W_f/W) with dedicated weak interface have been prepared by powder metallurgy process, combing the advantages of superb damage resilience with a much easier production compared to conventional chemical vapor deposition process. In this work, the newly developed material is characterized, including, mechanical tests, high heat flux tests, exposure to plasma for erosion and fuel retention tests. The L-W_f/W composite could improve significantly the damage resilience compared to pure W without altering much of other properties.

1. Introduction

For use as an armor material (PFM) in future fusion reactors, candidates require advanced mechanical and thermal properties to address the challenges caused by extreme fusion environments [1]. This is particularly true for the divertor region, where surfaces are exposed to intense particle and heat fluxes [2,3]. Tungsten is one of the most suitable materials for use as a PFM in the divertor region due to its favorable physical properties, such as low erosion rate, high sputtering threshold, high thermal conductivity, and high melting point [4,5]. However, the intrinsic brittleness of tungsten materials is a big concern for their application in fusion reactors [6,7]. The operational window is getting smaller when tungsten materials are exposed to fusion plasma with neutron irradiation (neutron embrittlement) [8]. Intensive efforts are being made to overcome the brittleness of tungsten or to improve its fracture toughness. One such approach involves tungsten fiber-reinforced tungsten composites (W_f/W) [9–13].

Similar to fiber-reinforced ceramic composites, the advanced mechanical properties of W_f/W do not only depend on the intrinsic mechanical properties of the fibers [14] but also on the energy dissipation during crack propagation, which is generated by the interaction between the W fibers and the W matrix [15,16]. One of the crucial factor is the existence of a dedicated interface between the fiber and matrix [15]. Based on these energy dissipation mechanisms, crack tips can be passivated, and crack propagation can be constrained. These mechanisms work even with a brittle matrix and fibers, as long as an engineered interface exists between the fiber and matrix. As a result, W_f/W exhibits, in contrast to pure tungsten, "pseudo-ductility" and

* Corresponding author.
E-mail address: y.mao@fz-juelich.de (Y. Mao).

https://doi.org/10.1016/j.fusengdes.2025.115605
Received 8 January 2025; Received in revised form 10 December 2025; Accepted 23 December 2025

significantly enhanced fracture toughness even after neutron irradiation [17–19].

W materials are primarily produced by powder metallurgical processes. Field assisted sintering technology (FAST), as a mature powder metallurgy process, is a pressure-assisted sintering synthesis technology using low-voltage pulsed direct current [20]. Recently, a novel type of aligned long fiber W_f/W (L-W_f/W) has been developed based on the FAST process, demonstrating excellent mechanical performance, combining with a rather convenient production process [13]. In this study, the application of this newly developed L-W_f/W as plasma-facing material is further demonstrated. Beyond mechanical properties, other application-relevant characteristics have been characterized, including resistance against cyclic loading, high-temperature mechanical properties, hydrogen retention characteristics, plasma erosion properties, and resistance against transient heat flux.

2. Experiments

2.1. Sample preparation

The preparation method of the L-W_f/W is adapted from the method described in [13]. The raw materials used were W weaves and W powders. The W weaves were woven by the institute of Textile Technology (ITA), RWTH Aachen Univeristy, using warp wires of 150 μm diameter and weft wires of 50 μm diameter. The W weaves were designed with a warp fiber spacing of 200 μm for mechanical reinforcement, while the weft fibers, spaced at 2 mm, served primarily to stabilize the weave. The wires possess an elongated grain structure resulting from a drawing process. Due to the elongated grain structures, the tensile strength of the wire used is up to 3000 MPa with a ductility above 3 % plastic deformation [21]. The W weaves were laser-cut into circular shapes with a diameter of 39 mm.

To establish a fiber/matrix interface, the weaves were coated with yttrium oxide (yttria). Yttria is used here as the interface material due to its excellent thermal and chemical stability and low neutron activation. The coating was applied using a magnetron sputtering process with a thickness of 2.5 μm, following the procedure outlined in [22].

A total of 20 layers of coated W weaves were alternated with 21 layers of W powders in a graphite sintering mold (40 mm in diameter). A protective W foil was used between the graphite mold and the green body to reduce the carbon contamination [23]. Approximately 4 g of W powder was evenly spread between each layer of W weave to cover the weave surface during packing. In contrast to the samples described in [13], which featured warp wires aligned in a single direction, the weave layers in the present work were alternately stacked at 0° and 90°, producing a bidirectional fiber orientation. In this way, the composite can have a two-directional reinforcement.

The consolidation of the stacked green body was performed with a Field Assisted Sintering Technology (FAST). The process was carried out under vacuum (<0.1 mbar) at 1850 °C with a pressure of 50 MPa, a holding time of 5 min, and a heating speed of 100 °C/min. A disc shape sample with bidirectional continuous fibers was produced as a result. The relative density of the samples after FAST consolidation is around 91 % based on Archimedes principle. Here, the sintering parameters were intentionally limited to avoid excessive temperature and prolonged holding time, which would lead to fiber recrystallization and consequently degrade the mechanical performance of the composite. Therefore, the obtained density of ~91 % represents a balance between matrix consolidation and preservation of the fiber's mechanical integrity. This density is close to the upper limit achievable without compromising the fiber microstructure. In future work, we plan to further optimize the sintering parameters to increase the composite density while maintaining the fiber's grain structure.

2.2. Mechanical testing

To investigate the fracture behavior and performance under various conditions, bending tests were conducted on L-W_f/W samples after sintering. The test specimens were prepared following the EU standards DIN EN ISO 148–1 and 14,556: 2006–2010 [24]. Small-sized specimens with KLST geometry were fabricated with dimensions of 27 mm × 3 mm × 4 mm (length × width × thickness), a span of 25 mm, a 1 mm V-notch depth, and a 0.1 mm notch root radius [25]. The specimens were cut using electrical discharge machining (EDM) without any additional surface or notch treatments.

The bending tests at room temperature were carried out using a universal testing device (TIRAtest 2820, Nr. R050/01, TIRA GmbH, Schalkau, Germany) at a constant testing speed of 1 μm/s. An optical camera system (DU657M Toshiba, Tokyo, Japan) was employed during these tests to monitor crack initiation and propagation behavior and to measure the absolute sample displacement. Here, the sample displacement is defined as the vertical movement of the sample relative to the reference stage. Concurrently, the corresponding force was recorded, enabling the generation of a force-displacement curve for each test.

In addition to the tests at room temperature, 3-point bending tests were also performed on KLST-type samples at elevated temperatures of 500 °C and 1000 °C at Universidad Politécnica de Madrid. These tests were conducted in a vacuum environment to prevent oxidation and maintain material integrity under high-temperature conditions with the same testing parameters as the room-temperature tests. However, the displacement during these tests was not directly measured; instead, it was determined based on the movement of the testing machine.

To evaluate the behavior of L-W_f/W under cyclic loading conditions, which simulate thermal stresses encountered during operational cycles, a 3-point bending test with cyclic loading was performed on KLST-type specimens. Initially, the stress was increased until the onset of matrix cracking. Subsequently, the samples were subjected to cyclic loading between 150 N and 250 N for 10,000 cycles. Following the cyclic loading phase, the test was concluded by breaking the sample.

2.3. Erosion by plasma

To investigate the erosion resistance by plasma, L-W_f/W and reference pure W were exposed to Ne plasma in linear plasma device PSI-2 [26] with the sample temperature controlled by water cooling. The sample temperature during Ne plasma exposure was monitored by a thermo couple attached to the backside of the sample. Both samples were exposed in the same experiment next to each other. The incident energy of Ne ions was 110 eV; the total exposure fluence was 3×10^{24} Ne^{+} m^{-2}. The plasma parameters were measured by Langmuir probe. There are typically a few percent Ne^{2+}in the neon discharge [27]. As Ne^{2+}has double incident energy, it could slightly contribute to the sputtering, but it was not considered in the calculation later on, as both samples were tested in the same discharge. During the exposure, the sample temperature was ~90 °C.

The sample masses before and after Ne plasma exposure were measured by micro-balance to assess the mass loss caused by the plasma erosion. The evolution of sample surface morphology due to erosion was characterized using scanning electron microscope (SEM, Zeiss DSM 982). Before plasma erosion, a focused ion beam (FIB) cut cross section was created on the sample surface with line marking. The same cross section was tracked after plasma erosion. By comparing the removed marking lines, the surface depth removed can be measured [28].

2.4. Deuterium retention

Another set of samples (including L-W_f/W and reference W) were exposed to Deuterium (D) plasma in PSI-2 to study the retention behavior of hydrogen isotopes in L-W_f/W. Both samples were exposed in the same experiment next to each other. The incident energy of D ions

was 95 eV; the total fluence was 5×10^{25} D^{+} m^{-2}. During the exposure, the sample temperature was controlled at around 275 °C.

After the exposure to D plasma, the samples were analyzed by Nuclear Reaction Analysis (NRA) at the Max Planck Institute for Plasmaphysics, Garching Germany. The NRA measurements were conducted with a ^{3}He beam of 1 mm × 1 mm spot size. Lateral scans were performed at 2.4 MeV with a 1 mm step width, providing an information depth of <3.3 μm. Depth profiling was carried out using six different ^{3}He energies, ranging from 690 keV to 4.5 MeV, enabling the probing of deuterium within the first 7.5 μm of the sample surface. High energy protons from the reaction were detected with solid state detectors under a reaction of 135° with large solid angle to achieve good counting statistics and with an annular detector under 175° with good depth resolution. At energies < 1200 keV a solid state detector placed at a reaction angle of 102° was used to detect the low energy alpha particles. Backscattered ^{3}He was detected under 165° for charge quantification, and a detector at 102° for alpha particles. The NRADC [29] software was used together with SIMNRA 7.04 [30] to deconvolute all measured proton and alpha spectra simultaneously and derive the most probable depth profile. Cross section data from Wielunska et al. was used [31].

2.5. Laser thermal shock experiments

To investigate the materials behavior under transient heat load condition, laser beam exposure was applied in PSI-2. A Nd:YAG laser (LASAG FLS 352 N, λ = 1064 nm) was used, with absorbed power densities between 0.19 GW/m^2 and 1.6 GW/m^2 [7]. A circular area with a diameter of 3.6 mm was exposed with a pulse frequency of 0.5 Hz in order to allow sample cooling down to room temperature after each pulse. For each sample, 4 spots were tested with different power densities, pulse numbers or durations: a. 0.19 GW/m^2, 100 pulses, 1 ms; b. 0.38 GW/m^2, 100 pulses, 1 ms; c. 0.38 GW/m^2, 1000 pulses, 1 ms; d. 1.6 GW/m^2, 1 pulse, 2 ms. The surface morphology after the laser beam shock was analyzed by SEM.

3. Results and discussion

3.1. Microstructure and mechanical properties

After the sintering process, the microstructure of the W_f/W was analyzed by a Zeiss LEO 982 scanning electron microscope (SEM, Jena, Germany). The typical microstructure is shown in Fig. 1. As can be seen from the Fig. 1, each weave layer is oriented perpendicular to its adjacent layers. The fiber volume fraction is around 25 %. The fiber volume fraction (~25 %) was estimated from optical images analyzed using ImageJ software over three representative cross-sectional areas (each ~5 mm^2). Local variations exist due to the woven architecture and the manual preparation, but the fiber distribution is macroscopically homogeneous across the specimen. The yttrium oxide interface is still visible after sintering, enclosing the fibers (the black ring around the fibers). In some local regions, the interface layer appears discontinuous. This can be attributed to several factors, likely acting in combination: (a) partial detachment of the thin yttria coating during the FAST process due to the high temperature and current; (b) local inhomogeneity of the yttria coating; and (c) minor damage introduced during handling and stacking of the coated weaves prior to sintering.

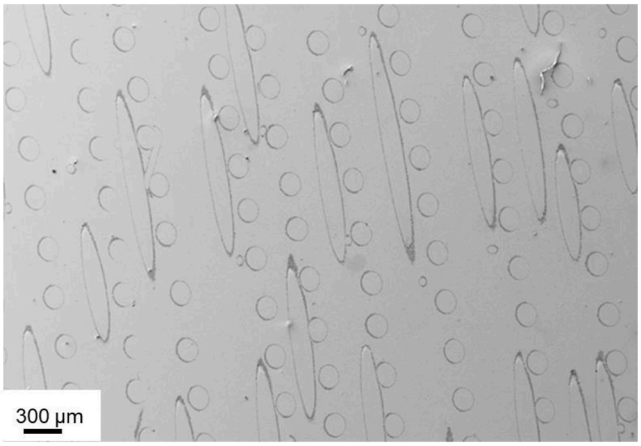

Fig. 1. Microstructure overview of L-W_f/W sample with 0–90° fiber orientation.

The mechanical properties of the L-W_f/W composite were characterized using in-situ 3-point bending tests at room temperature. The force-displacement curves for typical L-W_f/W and reference W samples are shown in Fig. 2. It can be seen that a pseudo ductile behavior with stable crack growth can be established by L-W_f/W samples: after a linear-elastic deformation, the slope of the curve changes gradually to negative values after several small load drops; after reaching the maximum force, the samples tend to have a continuous load-decreasing. Even after large deformation, the sample is still able to withstand a loading force of about 150 N. Compared to pure W, L-W_f/W represents a greatly improved damage resilience as indicated already in [13].

To evaluate the response of the L-W_f/W composite under conditions that simulate operational cyclic thermal stresses, cyclic loading tests were performed. The force-displacement curves of the cyclic loading are presented in Fig. 3. As it can be deduced from the curve, even though the cyclic loading is subjected after initial cracking of the matrix, the material could still hold 10^4 cycles without any sign of material degradation. For brittle pure W, a catastrophic failure would have already occurred in the first loading (crack initiation).

The mechanical behavior of L-W_f/W composite was evaluated also through 3-point bending tests conducted at elevated temperatures (500 °C and 1000 °C). As shown in Fig. 4(a), the force-displacement curves, all samples exhibited a pseudo-ductile behavior, characterized by a gradual decrease in load after reaching the maximum force, without catastrophic failure. With increasing testing temperature, the maximum force firstly increased at 500 °C. This could be due to the increasing of fiber ductility or matrix toughening, which will be investigated in the future. At 1000 °C, the maximum loading force decreased significantly compared to the tests at 500 °C and RT. This can be attributed to the softening of tungsten fibers at high temperatures. As shown in Fig. 4(b), a pronounced necking effect occurred in the tungsten fibers after failure at 1000 °C. This strong necking indicates significant plastic deformation of the fibers under the combined effects of high temperature and mechanical loading. For all the samples, the matrix fractured in a brittle manner. The matrix strength changing with increasing temperature is not investigated here, which could also result in the reducing of the

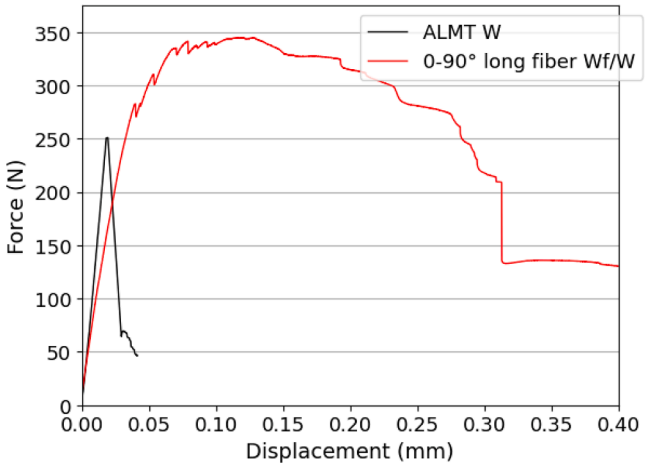

Fig. 2. Force-displacement curves of 3-point bending tests on KLST type samples for typical L-W_f/W and reference W.

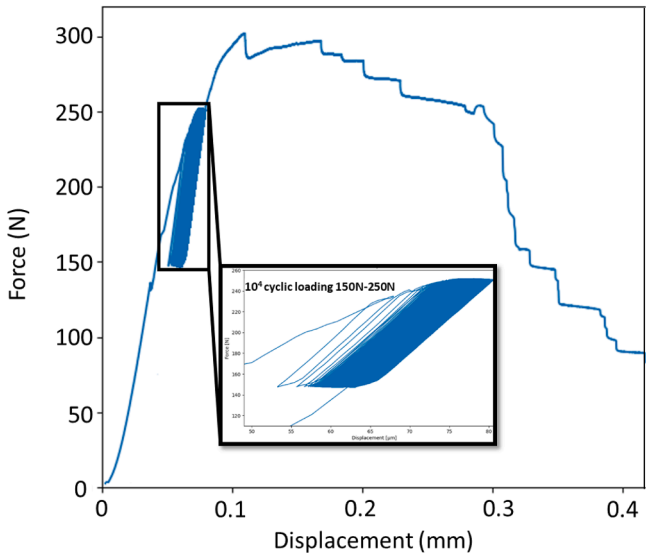

Fig. 3. Force-displacement curves of 3-point bending tests on KLST type samples for typical L-W_f/W with 10^4 cycles loading.

maximum loading force. Despite this, the composites maintained their pseudo-ductile behavior, demonstrating the toughening mechanisms even under elevated temperature conditions.

3.2. Plasma erosion properties

Ne plasma exposure experiments were conducted on both L-W_f/W composite and ITER-grade W (ITG-W) to assess their erosion behavior under plasma loading conditions. For L-W_f/W, the mass loss was approximately 3.06 mg, with an erosion depth of ~2.2 μm, while pure tungsten exhibited a mass loss of ~2.85 mg and an erosion depth of ~2.4 μm.

Assuming a normal incidence for all the impacting particles, the theoretical mass loss from a flat surface due to plasma sputtering can be calculated by [32]:

$$\Delta m_{weight} = \Phi \cdot Y \cdot S \cdot m_W \quad (1)$$

Where Δm_{weight} is the theoretical mass loss, Φ the incident particle fluence, Y the sputtering yield at given ion energy, S the surface area, m_W the mass of the tungsten atom.

Applying the sputtering yield of W in [32], the theoretical mass loss of pure W during the Neon plasma exposure is calculated as 3.3 mg. Both samples match within the experimental uncertainty compared to the theoretical value.

The results show that the mass loss and erosion depth are comparable for both types of samples. Although L-W_f/W composite contain yttria at the fiber-matrix interface, which has a higher sputtering yield compared to tungsten, the volume fraction of yttria is so small that, it had minimal influence on the overall erosion properties.

Fig. 5(a) illustrates surface morphology change before and after Ne plasma exposure together with a FIB cross-section of the L-W_f/W composites and the line markings used to measure the depth loss before and after plasma erosion. The cross-section here was cut at a fiber interface region. Post-erosion observations reveal that the tungsten fiber in the examined region was nearly completely eroded.

Although the volume fraction of yttria is small, its lower density compared to W means that the mass-based erosion analysis underestimates its contribution. While its sputtering is likely preferential, the impact on total mass loss is negligible. Microscopically, the removal of the interface happens mainly at the surface and would not so much affect local mechanical integrity and thermal stability. But further study will be performed in the future.

3.3. Deuterium retention

The deuterium (D) retention behavior of the L-W_f/W and pure ITER-grade W (ITG-W) was studied using NRA after exposure to D plasma in PSI-2. Fig. 6(a) shows an NRA line scan through the L-W_f/W sample and a pure W reference sample, illustrating the NRA signal dependence across different positions on the surface. For the L-W_f/W sample, the left portion of the surface has fibers exposed at the surface, while the right portion reveals only the matrix. This surface characteristic arises from the slight misalignment of weave layers during sample preparation. Although unintentional, this feature enabled the measurement of retention property difference fibers and matrix. As seen in the Fig. 6(a), the fiber region exhibits higher D retention compared to the pure W, which could be attributed to the higher defect density in the fibers [33] from the extremely elongated grain structure. Furthermore, the matrix region demonstrates even higher D retention potentially due to its higher closed porosity, which provides additional trapping sites for D atoms.

Fig. 6(b) presents the depth profiles for the open circle positions in

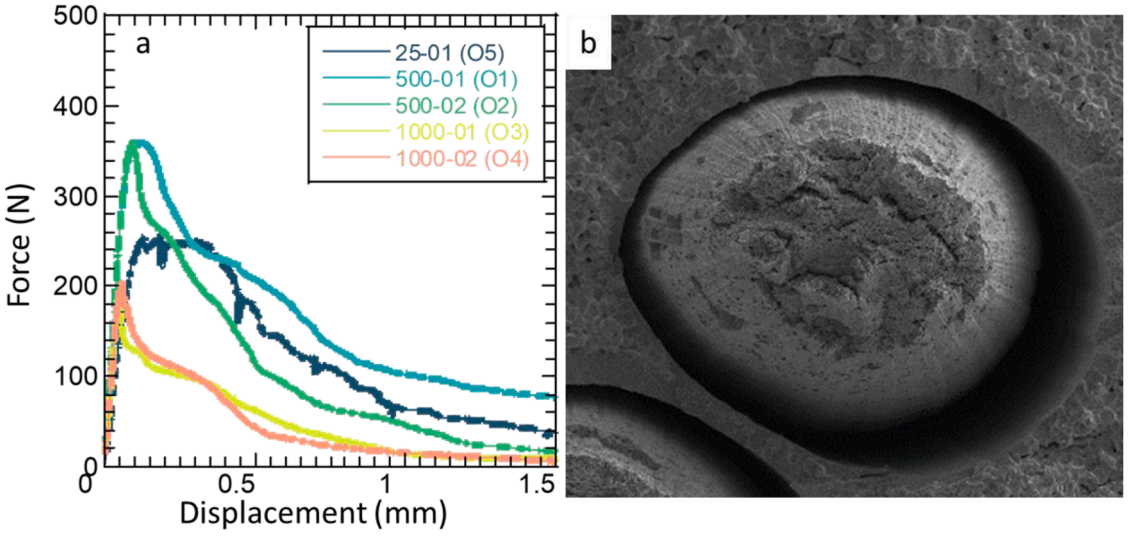

Fig. 4. (a) Force displacement curves of the 3-point bending tests on W_f/W with KLST geometry at different temperatures, in total there are 5 samples tested O1-O5; (b) fiber fracture section of the sample tested at 1000 °C.

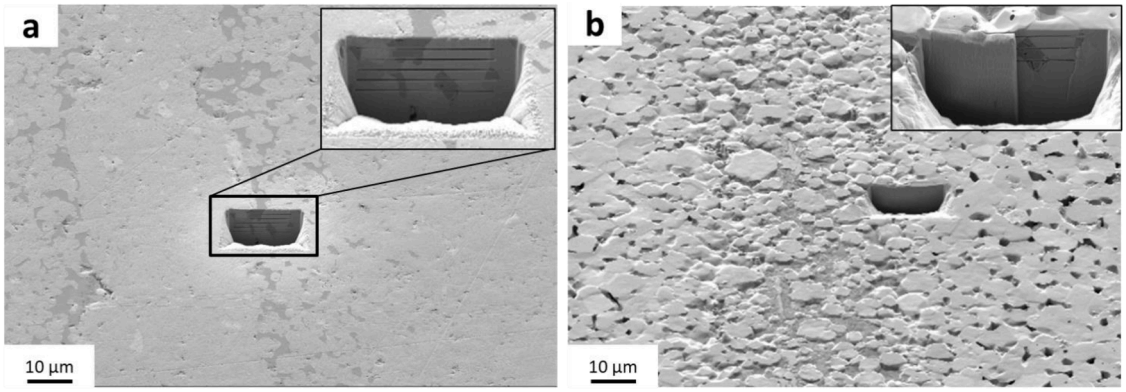

Fig. 5. W_f/W surface morphology before (a) and after (b) Ne plasma erosion, with FIB cut cross section and line marking to track the depth removal; the picture on the right top corners show the line marks on the cross section; the cross section after erosion test need to be cleaned up by FIB to remove the redeposition layer.

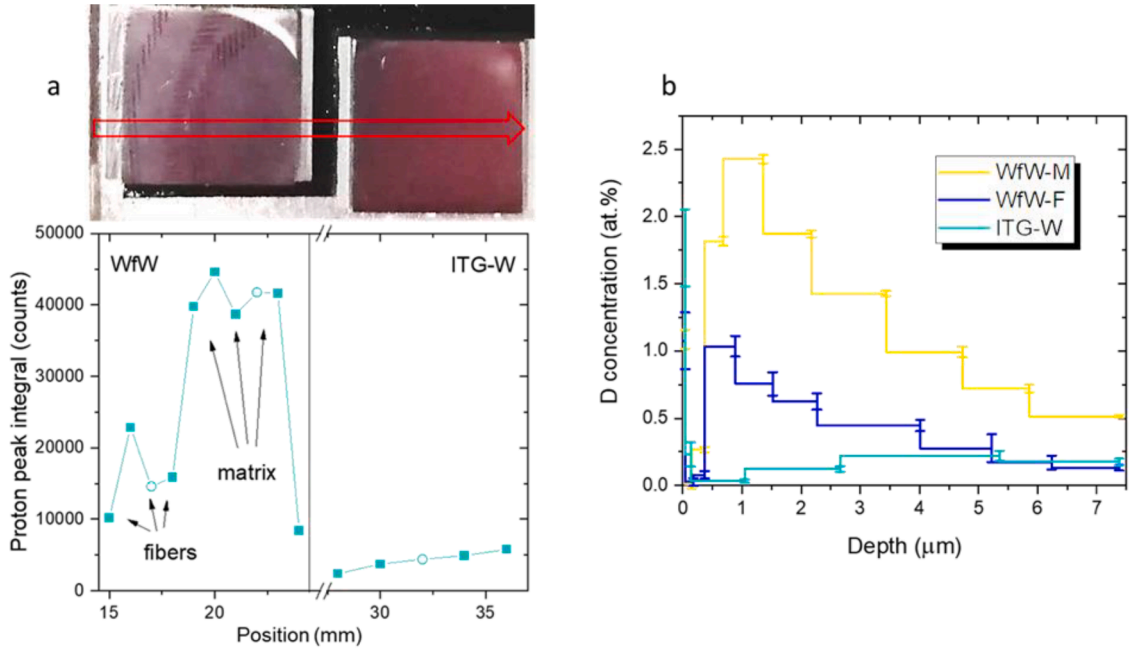

Fig. 6. NRA analysis on W_f/W and reference W after D plasma exposure to measure the D retention. (a) line scan on W_f/W and reference (b) D concentration depth profile on the W matrix, the W fibres and the ITG-W (open circles indicated in (a)).

Fig. 6(a). The depth range measured here is 7 μm, which is still quite shallow compared to the fiber dimension. So the measurement is very likely still within the fiber and matrix respectively. These profiles confirm the same trends observed in the surface scan, with the matrix region retaining the highest amount of deuterium, followed by the fiber region, and then pure W. However, the retention differences between these regions narrow with increasing depth, as the surface-dominated effects diminish. The total D concentrations for the first 7 μm by integrating the curves results in a D content of 5.4E21 D/m^2 for the W_f/W matrix region, 1.7E21 D/m^2 for the W_f/W fiber region and 0.8E21 D/m^2 for reference W, respectively. This reveals that the retention differences among the regions are less than one order of magnitude, indicating that the variation is still relatively moderate.

3.4. Laser shock experiments

The laser shock tests were performed to evaluate the behavior of L-W_f/W composite in comparison to pure ITER-grade W under transient high heat load conditions. Four exposure sequences were applied to each type of sample at varying power densities and pulse numbers as described in experimental section. Low-power tests (0.19 and 0.38 GW/m^2) did not cause any cracking for either material. However, the highest power test (1.6 GW/m^2) resulted in significant surface cracking due to thermal stress, as shown in Fig. 7 for both materials. The L-W_f/W samples exhibited a lower total crack length compared to pure W. The crack density is estimated by the total crack length within the tested area. For the reference W, the total crack length is ~ 20 mm and the Wf/W ~ 11 mm. As can be observed from the crack pattern on L-W_f/W surface, due to the existence of the fibers and the weak interface, the cracks were deflected. The red-marked area shows that the crack direction changes along the weak interface and that the interface opens, demonstrating the effectiveness of the extrinsic toughening mechanism. These mechanisms absorbed extra energy during crack propagation, thereby leading to mitigated damage. In contrast, cracks in pure tungsten propagated directly across the material without significant deviation, leading to a higher total crack length. These results show the better resilience of the L-W_f/W composite under transient high thermal stress conditions.

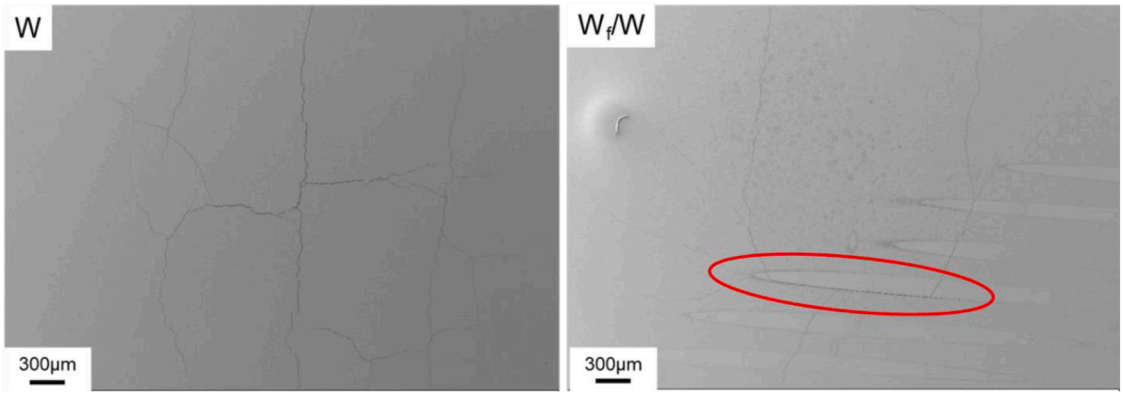

Fig. 7. Surface morphology of reference W and W_f/W after a laser shock test with 1.6 GW/m^2 for 2 ms.

4. Summary and conclusion

The newly developed powder-metallurgical long tungsten fiber-reinforced tungsten composite (L-W_f/W) has been characterized, including its mechanical behavior, plasma erosion resistance, hydrogen isotope retention, and high heat flux performance under laser shock.

Mechanical testing, including 3-point bending tests conducted at room and elevated temperatures, confirmed that L-W_f/W composite exhibit pseudo-ductile behavior. At elevated temperatures up to 1000 °C, the W_f/W retained its pseudo-ductile characteristics, but the maximum load decreased due to fiber softening. Under cyclic loading, L-W_f/W maintained their structural integrity for over 10,000 cycles, underlining its fatigue resistance.

Plasma erosion tests revealed that the erosion resistance of L-W_f/W is comparable to that of pure W. The retention behavior of deuterium in L-W_f/W composite revealed a more complex material characteristics. The fiber regions exhibited higher retention compared to pure W and the matrix regions showed even higher retention probably due to their higher porosity. However, the differences in retention narrowed with increasing depth, remaining below one order of magnitude. Laser shock testing under transient high heat flux conditions showed that L-W_f/W composite displayed less surface cracking compared to pure W. This behavior could be attributed to the energy dissipation mechanisms provided by the introduction of fibers and weak interfaces within the composite, which effectively deflect cracks and mitigate damage.

In summary, L-W_f/W composite significantly improves damage resilience compared to pure tungsten, while maintaining comparable erosion resistance and manageable retention levels for hydrogen isotopes, which makes L-W_f/W a promising candidate for use as PFM in future fusion reactors.

CRediT authorship contribution statement

Yiran Mao: Writing – review & editing, Writing – original draft, Methodology, Investigation, Formal analysis, Data curation, Conceptualization. **Jan Willem Coenen:** Writing – review & editing, Validation, Supervision, Project administration, Conceptualization. **Johann Riesch:** Writing – review & editing, Validation, Project administration, Methodology, Investigation, Conceptualization. **Thomas Schwarz-Selinger:** Writing – review & editing, Visualization, Methodology, Investigation. **Elena Tejado:** Writing – review & editing, Validation, Methodology, Investigation. **Arkadi Kreter:** Writing – review & editing, Validation, Methodology, Investigation, Data curation. **Alexis Terra:** Methodology, Investigation, Conceptualization. **Marius Wirtz:** Methodology, Investigation, Conceptualization. **Marcin Rasinski:** Methodology, Investigation. **Juan Du:** Writing – review & editing, Methodology. **Xiaoyue Tan:** Methodology. **Yaohui Liu:** Methodology. **Rudolf Neu:** Supervision, Resources, Project administration. **Christoph Broeckmann:** Supervision, Resources, Project administration. **Christian Linsmeier:** Supervision, Resources, Funding acquisition.

Declaration of competing interest

The authors declare that they have no known competing financial interests or personal relationships that could have appeared to influence the work reported in this paper.

Acknowledgement

This work has been carried out within the framework of the EUROfusion Consortium, funded by the European Union via the Euratom Research and Training Programme (Grant Agreement No 101052200 - EUROfusion). The authors also acknowledge the support of Dr. Liang Gao for his helpful insights into the interpretation of the NRA results.

Data availability

Data will be made available on request.

References

[1] U. Schumacher, Status and problems of fusion reactor development, Naturwissenschaften. 88 (3) (2001) 102–112.
[2] H. Bolt, V. Barabash, W. Krauss, J. Linke, R. Neu, S. Suzuki, et al., Materials for the plasma-facing components of fusion reactors, J. Nucl. Mater. (2004) 329–333, 66-73.
[3] M. Merola, D. Loesser, A. Martin, P. Chappuis, R. Mitteau, V. Komarov, et al., ITER plasma-facing components, Fusion Eng. Des 85 (10–12) (2010) 2312–2322.
[4] V. Philipps, Tungsten as material for plasma-facing components in fusion devices, J. Nucl. Mater. 415 (1) (2011) S2–S9.
[5] J.W. Coenen, S. Antusch, M. Aumann, W. Biel, J. Du, J. Engels, et al., Materials for DEMO and reactor applications—Boundary conditions and new concepts, Phys. Scr. (T167) (2016) 014002, 2016.
[6] G. Pintsuk, I. Bobin-Vastra, S. Constans, P. Gavila, M. Rödig, B. Riccardi, Qualification and post-mortem characterization of tungsten mock-ups exposed to cyclic high heat flux loading, Fusion Eng. Des 88 (9–10) (2013) 1858–1861.
[7] A. Huber, A. Arakcheev, G. Sergienko, I. Steudel, M. Wirtz, A. Burdakov, et al., Investigation of the impact of transient heat loads applied by laser irradiation on ITER-grade tungsten, Phys. Scr. (T159) (2014) 014005, 2014.
[8] H. Bolt, V. Barabash, G. Federici, J. Linke, A. Loarte, J. Roth, et al., Plasma facing and high heat flux materials - needs for ITER and beyond, J. Nucl. Mater. (2002) 43–52, 307-3111 SUPPL.
[9] J. Riesch, J.Y. Buffiere, T. Höschen, M. di Michiel, M. Scheel, C. Linsmeier, et al., In situ synchrotron tomography estimation of toughening effect by semi-ductile fibre reinforcement in a tungsten-fibre-reinforced tungsten composite system, Acta Mater. 61 (19) (2013) 7060–7071.
[10] Y. Mao, J.W. Coenen, J. Riesch, S. Sistla, J. Almanstotter, B. Jasper, et al., Influence of the interface strength on the mechanical properties of discontinuous tungsten fiber-reinforced tungsten composites produced by field assisted sintering technology, Compos. Part a-Appl. S 107 (2018) 342–353.
[11] H. Gietl, J. Riesch, J.W. Coenen, T. Hoschen, C. Linsmeier, R. Neu, Tensile deformation behavior of tungsten fibre-reinforced tungsten composite specimens in as-fabricated state, Fusion Eng. Des 124 (2017) 396–400.
[12] J. Du, J.-H. You, T. Höschen, Thermal stability of the engineered interfaces in Wf/W composites, J. Mater. Sci. 47 (11) (2012) 4706–4715.

[13] Y. Mao, J.W. Coenen, C. Liu, A. Terra, X. Tan, J. Riesch, et al., Powder metallurgy produced aligned long tungsten fiber reinforced tungsten composites, J. Nuclear Eng 3 (4) (2022) 446–452.
[14] J. Riesch, Y. Han, J. Almanstotter, J.W. Coenen, T. Hoschen, B. Jasper, et al., Development of tungsten fibre-reinforced tungsten composites towards their use in DEMO-potassium doped tungsten wire, Phys. Scr. (T167) (2016) 014006. T167.
[15] R. Shu, Y. Mao, J.W. Coenen, A. Terra, C. Liu, S. Schönen, et al., Interface and mechanical properties of the single-layer long fiber reinforced wf/W composites fabricated via field assisted sintering technology, Mater. Sci. Eng 857 (2022) 144098.
[16] Y. Mao, J.W. Coenen, J. Riesch, S. Sistla, J. Almanstötter, B. Jasper, et al., Development and characterization of powder metallurgically produced discontinuous tungsten fiber reinforced tungsten composites, Phys. Scr. 70 (2017) 014005. T1.
[17] Y. Mao, J.W. Coenen, J. Riesch, S. Sistla, J. Almanstötter, J. Reiser, et al., Fracture behavior of random distributed short tungsten fiber-reinforced tungsten composites, Nucl. Fusion 59 (8) (2019) 086034.
[18] H. Gietl, J. Riesch, M. Zielinski, T. Höschen, J.W. Coenen, S. Schönen, et al., Interlayer properties of tungsten fibre-reinforced composites and their determination by different methods, Nuclear Mater. Energy (2021) 28.
[19] T. Höschen, A. Zinovev, C. Chang, D. Terentyev, H. Gietl, Y. Mao, et al., Results of the EUROfusion irradiation campaign for Wf/W material, 20th Int. Conf. Fusion Reactor Mater. (ICFRM–20) (2021).
[20] O. Guillon, J. Gonzalez-Julian, B. Dargatz, T. Kessel, G. Schierning, J. Räthel, et al., Field-assisted sintering technology/spark plasma sintering: mechanisms, materials, and technology developments, Adv. Eng. Mater. 16 (7) (2014) 830–849.
[21] J. Riesch, J. Almanstötter, J.W. Coenen, M. Fuhr, H. Gietl, Y. Han, et al., Properties of drawn W wire used as high performance fibre in tungsten fibre-reinforced tungsten composite, IOP Conf. Series 139 (2016) 012043.
[22] Y. Mao, J. Engels, A. Houben, M. Rasinski, J. Steffens, A. Terra, et al., The influence of annealing on yttrium oxide thin film deposited by reactive magnetron sputtering: process and microstructure, Nuclear Mater. Energy 10 (2017) 1–8.
[23] Y. Mao, C. Chen, J. Coenen, J. Riesch, S. Sistla, J. Almanstötter, et al., On the nature of carbon embrittlement of tungsten fibers during powder metallurgical processes, Fusion Eng. Des 145 (2019) 18–22.
[24] Prüfung metallischer Werkstoffe; Kerbschlagbiegeversuch; Besondere Probenform und Auswertungsverfahren, s.l, in: DIN, 50115, Beuth-Verlag, 1991.
[25] M. Rieth, A. Hoffmann, Influence of microstructure and notch fabrication on impact bending properties of tungsten materials, Int. J. Refract. Met. Hard. Mater 28 (6) (2010) 679–686.
[26] A. Kreter, C. Brandt, A. Huber, S. Kraus, S. MÖller, M. Reinhart, et al., Linear plasma device PSI-2 for plasma-material interaction studies, Fusion Sci. Technol 68 (1) (2015) 8–14.
[27] I.A. Sorokin, I.V. Vizgalov, V.A. Kurnaev, C. Brandt, A. Kreter, C. Linsmeier, In-situ mass-spectrometer of magnetized plasmas, Nuclear Mater. Energy 12 (2017) 1243–1247.
[28] M. Rasiński, S. Brezinsek, A. Kreter, T. Dittmar, K. Krieger, M. Balden, et al., FIB line marking as a tool for local erosion/deposition/fuzz formation measurements in ASDEX Upgrade during the He campaign, Nuclear Mater. Energy 37 (2023).
[29] K. Schmid, U. von Toussaint, Statistically sound evaluation of trace element depth profiles by ion beam analysis, Nuclear Instrum. Methods Phys. Res. Sec. B 281 (2012) 64–71.
[30] M. Mayer, S. Möller, M. Rubel, A. Widdowson, S. Charisopoulos, T. Ahlgren, et al., Ion beam analysis of fusion plasma-facing materials and components: facilities and research challenges, Nucl Fusion 60 (2) (2020).
[31] B. Wielunska, M. Mayer, T. Schwarz-Selinger, U. von Toussaint, J. Bauer, Cross section data for the D(3He,p)4He nuclear reaction from 0.25 to 6 MeV, Nuclear Instrum. Methods Phys. Res. Sec. B 371 (2016) 41–45.
[32] W. Eckstein, Calculated sputtering, Reflection and Range Values, Max-Planck-Institut für Plasmaphysik, Germany, 2002, p. 313.
[33] A. Kärcher, J. Riesch, P. Almanstötter, A. Manhard, M. Balden, J.W. Coenen, et al., Deuterium retention in tungsten fiber-reinforced tungsten composites, Nuclear Mater. Energy (2021) 27.